JOURNAL OF CATALYSIS 139, 351–361 (1993)

Acidity and Catalytic Activity of MeAPSO-44 (Me = Co, Mn, Cr, Zn, Mg), SAPO-44, $AlPO_4$-5, and $AlPO_4$-14 Molecular Sieves in Methanol Dehydration

STANKO HOČEVAR, JURKA BATISTA, AND VENČESLAV KAUČIČ

Department of Catalysis and Chemical Reaction Engineering, Institute of Chemistry, Hajdrihova 19, P.O. Box 30, 61115 Ljubljana, Slovenia

Received March 13, 1992; revised July 23, 1992

SAPO-44 and the isomorphously substituted MeAPSO-44 (Me = Co, Mn, Cr, Zn, Mg) molecular sieves have been synthesized. The temperature-programmed desorption (TPD) spectra and the reaction rates of methanol dehydration have been measured on these samples in comparison with $AlPO_4$-5 and $AlPO_4$-14 samples. The acidity strength of samples has been determined qualitatively from the temperatures of dimethylether desorption peaks, and the following sequence has been obtained: MnAPSO-44 > CoAPSO-44 ≈ ZnAPSO-44 > MgAPSO-44 > CrAPSO-44 > SAPO-44 ≫ $AlPO_4$-5 ≈ $AlPO_4$-14. The following sequence of catalytic activity has been observed: $AlPO_4$-14 > $AlPO_4$-5 ≈ SAPO-44 > CoAPSO-44 > MnAPSO-44. The highest selectivity to ethene production among these catalysts has been found for CoAPSO-44. The selectivities to ethene of SAPO-44 and MeAPSO-44 (Me = Co, Mn, Cr) samples are about three times higher than the selectivities of SAPO-34 and MeAPSO-34 (Me = Co, Mn, Cr) samples. The selectivities of transition-metal-substituted MeAPSO-44 samples follow the Irving–Williams transition metal–ligand complex stability order.

INTRODUCTION

In view of the several papers published recently by different authors in which they claim the unique selectivity of the SAPO-34 and NiAPSO-34 molecular sieves toward ethene in the methanol-to-olefins reaction (*1–4*), it seemed to us interesting to compare the acidity, catalytic activity, and selectivity of the SAPO-34, MeAPSO-34 and SAPO-44, MeAPSO-44 molecular sieves in the same reaction. Both -34 and -44 structural types have chabazite-like topology, but they differ in lattice symmetry (*5–7*).

In a preceding paper (*8*) one of us presented results on the acidity and catalytic activity of SAPO-34, MeAPSO-34 (Me = Co, Mn, Cr), and H-ZSM-5 molecular sieves in methanol dehydration. It was shown there how isomorphously substituted elements influence the acidity strength of MeAPSO-34 molecular sieves and consequently the selectivity toward ethene formation. The present paper broadens this discussion on the influence of the structure of MeAPSO molecular sieves on the selectivity. For this purpose SAPO-44, MeAPSO-44 (Me = Co, Mn, Cr, Zn, Mg) were synthesized and their acidities, catalytic activities, and selectivities in the methanol dehydration reaction were compared with those of the -34 structural type homologues. $AlPO_4$-5 and $AlPO_4$-14 molecular sieves were used as the reference samples for acidity and catalytic activity measurements. The techniques used for characterization of samples with regard to acidity strength, catalytic activity, and selectivity for ethene formation in the methanol-to-olefins reaction were the same as in our previous study (*8*), i.e., TPD of methanol followed by TG/MS and catalytic activity, followed by reaction rate measurements in a gradientless catalytic reactor.

0021-9517/93 $5.00

EXPERIMENTAL

The SAPO-44, CoAPSO-44, MnAPSO-44, and ZnAPSO-44 samples were synthesized according to the procedures described in Refs. (*9–12*), respectively, CrAPSO-44 and MgAPSO-44 were synthesized as described in Ref. (*13*), and the $AlPO_4$-5 and $AlPO_4$-14, as reference samples, were prepared according to Ref. (*14*). All samples were characterized by means of X-ray powder diffraction (structural type, degree of crystallinity, phase purity), scanning electron microscopy (morphology, particle size, phase purity), thermogravimetry (content of the organic template and water, thermal stability of samples), and quantitative chemical analysis. The templates were removed from the as-synthesized samples by calcination at 823 K for 4 h in a flow of dry air. The calcined samples were pressed out in slabs of 30 mm in diameter and 1.5 mm thick at the pressure of 20.3 bars. The slabs of each sample in the amount of 0.89 g (on average per sample) were used for catalytic activity measurements in a gradientless catalytic reactor under reaction conditions described in Ref. (*8*). A fraction of the crushed slabs (0.2 to 0.3 mm) was used for temperature-programmed desorption (TPD) measurements. The apparatus and the procedure for these measurements are described in detail in a preceding paper (*8*).

RESULTS AND DISCUSSION

The chemical composition of samples and the framework charges calculated on the basis of the TO_2 formula (*15*) are given in Table 1.

Typical TPD traces of adsorbed methanol on SAPO-44 and CoAPSO-44 molecular sieves are shown in Figs. 1 and 2, respectively. The enhanced traces of dimethylether desorption peaks from the series of SAPO-44 and MeAPSO-44 molecular sieves are shown in Fig. 3.

The mass balance of TPD experiments is given in Table 2. As can be seen from this table the mass of adsorbed methanol equals, within the experimental error, the mass of evolved gases during TPD as measured by TG. The composition of desorbed products in molar fractions reveals that a substantial part of the methanol desorbs unconverted. The remainder of the methanol reacts through the formation of dimethylether (DME) at lower temperatures and further on through the formation of hydrocarbons at higher temperatures. However, the quantities of desorbed hydrocarbons are small, since these molecules are transformed within the chabazite cages through the hydrocarbon reactions to coke. All samples except $AlPO_4$-5 and $AlPO_4$-14 were overlaid by light to dark grey deposits of coke after TPD.

The mass balance of the methanol TPD process, calculated according to the procedure described in our previous paper (*8*), is given in Table 3. Here n represents the number of moles of adsorbed methanol per gram of sample, m represents the number of moles of desorbed products per gram of sample, χ_{CH_3OH} represents the conversion of methanol, and $\chi_{(CH_3)_2O}$ the conversion of dimethylether. The mass balance presented in Table 3 thus takes into consideration the fact that some water, the product of the fast surface-exchange reaction between adsorbed methanol and residual water on the molecular sieve surface at room temperature, desorbs at low temperature, and the fact that some methanol is converted during TPD into nondesorbable higher hydrocarbons and coke (*8*).

Table 4 contains the following data pertinent to the subsequent discussion: the concentration of isomorphously substituted elements (in moles per gram of catalyst) that build up the active centers of the type T_1–(OH)–T_2, where T_1 = Al, Co, Mn, Cr, Zn, Mg and T_2 = Si, P, respectively (*15*); the T–O bond distances of these elements in the aluminophosphate structures (*15*); the experimentally determined temperatures of dimethylether desorption peaks; the molar ratios of desorbed dimethylether to desorbed methanol, calculated from the data given in Table 2; and the reaction rates of

TABLE 1

The SAPO-44, MeAPSO-44, and $AlPO_4$-*n* Chemical Composition Calculated on TO_2 Basis

Sample	Me	Al	Si	P	Si + P	Framework charge
SAPO-44	—	0.50	0.14	0.36	0.50	−0.14
CoAPSO-44	0.04	0.46	0.11	0.39	0.50	−0.15
MnAPSO-44	0.04	0.44	0.15	0.37	0.52	−0.15
CrAPSO-44	0.01	0.49	0.17	0.33	0.50	−0.18
ZnAPSO-44	0.04	0.46	0.12	0.37	0.49	−0.16
MgAPSO-44	0.04	0.46	0.13	0.36	0.49	−0.17
$AlPO_4$-5	—	0.55	—	0.45	—	—
$AlPO_4$-14	—	0.52	—	0.48	—	—

methanol dehydration, calculated from the experimentally determined conversions of methanol in a gradientless reactor under the conditions described in Ref. (*8*).

Table 5 gives the selectivities for ethene obtained from TPD measurements as the weight percent of ethene in hydrocarbon products (coke included) normalized with respect to the concentration of desorbed species per gram of catalyst (calculated from the data in Table 3) and the selectivities as weight percent of ethene in hydrocarbon products (coke excluded) calculated from the product distribution obtained from the gradientless catalytic reactor.

Comparing the data on the mass balance of the TPD process from SAPO-44 and MeAPSO-44 samples (Table 2) with those from SAPO-34 and MeAPSO-34 samples reported in Table 2 of our preceding paper (*8*), we observe the following similarities or differences between these two series of samples:

—SAPO-44 has a lower quantity of adsorbed methanol than SAPO-34 sample in spite of the fact that the calculated framework charge on SAPO-44 is substantially higher than that on SAPO-34;

—CoAPSO-44 has a slightly higher quantity of desorbed species than CoAPSO-34 in spite of the fact that the Co loading in CoAPSO-34 is twice that in CoAPSO-44. However, on the other hand the Si loading in CoAPSO-44 is substantially higher than in CoAPSO-34;

—MnAPSO-44 has more than twice the quantity of adsorbed methanol as MnAPSO-

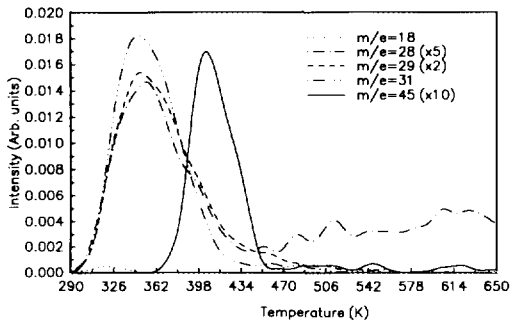

FIG. 1. TPD spectrum of methanol from SAPO-44 sample.

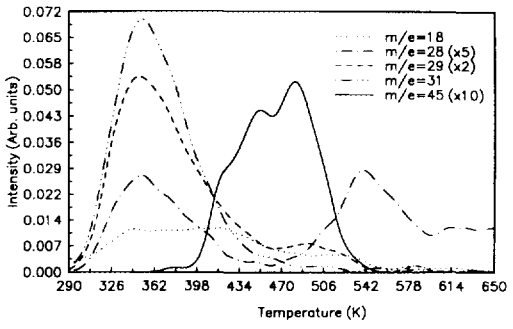

FIG. 2. TPD spectrum of methanol from CoAPSO-44 sample.

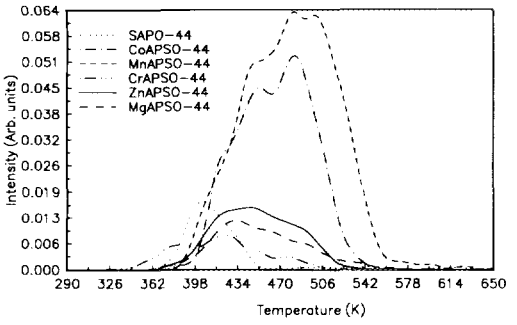

FIG. 3. Desorption peaks for fragmentary ion of dimethylether, m/e = 45 ($C_2H_5O^+$) (enhanced 10 times), observed in TPD spectra of methanol from molecular sieves.

34 despite the fact that Mn loading in both samples is equal. However, the loading of Si in MnAPSO-44 is much higher than that in MnAPSO-34;

—the quantities of adsorbed methanol on CrAPSO-44 and CrAPSO-34 are very close together, but the loading of Si in CrAPSO-44 is nearly twice that in CrAPSO-34;

—the quantity of adsorbed methanol in MgAPSO-44 is the highest one among all samples with -44-type structure. Also ZnAPSO-44 has a higher quantity of adsorbed methanol than the SAPO-44 and MeAPSO-44 (Me = Co, Mn, Cr) samples.

On the basis of this comparison one can hardly correlate the quantity of adsorbed methanol with either the loading of silicon or the loading of metal, or both of them. However, there are some other, very strong correlations that enable one to see more clearly what is happening during the methanol dehydration reaction on both series of molecular sieves. As we have already stated in the conclusions of our previous paper (*8*), the TPD experiment gives quantitative information about the acidity strength, catalytic activity, and selectivity of the catalysts.

The acidity strength is given by the temperatures of the DME desorption peaks during TPD of methanol (see Fig. 3). The correlation between the temperatures of the DME desorption peaks and the structural parameter of the catalysts, i.e., T–O bond distance, where T represents the isomorphously substituted elements (Si, Co, Mn, etc.), is shown in Fig. 4. The data from Fig. 8 in our preceding paper (*8*), related to the samples with -34 structural type, are also included in order to demonstrate that the acid strength depends only on the type of metal incorporated into the framework and not on the structural type (-34 or -44) of the aluminophosphate-based molecular sieves. The data on the quantity of methanol retained by molecular sieves after degassing at room temperature (Table 2) clearly demonstrate that

TABLE 2

Amount of Methanol Remaining Adsorbed after Degassing of Samples at 293 K; Quantity (TG) and Composition (MS) of Desorbed Species during TPD between 293 and 673 K

Sample	Methanol ads. (g/g)	Species des. (g/g)	Composition of des. prod. (molar fractions)			
			CH_3OH	H_2O	C_2H_4	$(CH_3)_2O$
SAPO-44	0.023	0.027	0.38	0.55	0.050	0.020
CoAPSO-44	0.049	0.039	0.61	0.25	0.080	0.050
MnAPSO-44	0.038	0.038	0.57	0.32	0.054	0.058
CrAPSO-44	0.018	0.018	0.43	0.46	0.020	0.080
ZnAPSO-44	0.051	0.050	0.65	0.26	0.083	0.010
MgAPSO-44	0.072	0.077	0.70	0.25	0.044	0.007
$AlPO_4$-5	0.010	0.011	0.06	0.94	0.000	0.000
$AlPO_4$-14	0.000	0.000	0.00	0.00	0.000	0.000

TABLE 3

Detailed Mass Balance of TPD Process and Conversions of Methanol and Dimethylether on SAPO-44 and MeAPSO-44 Molecular Sieves

	SAPO	CoAPSO	MnAPSO	CrAPSO	ZnAPSO	MgAPSO
n (mol/g)	0.72E-3	1.53E-3	1.19E-3	0.56E-3	1.59E-3	2.25E-3
m (mol/g)	0.94E-3	1.70E-3	1.57E-3	0.91E-3	1.81E-3	2.53E-3
			Products composition (wt% of CH_3OH adsorbed)			
CH_3OH	49.9	67.9	64.8	52.1	73.8	78.8
H_2O	26.7	14.8	16.1	21.4	14.2	11.5
$(CH_3)_2O$	3.7	8.3	9.4	14.3	1.5	1.1
C_2H_4	5.7	8.0	5.3	2.4	8.2	4.3
Residuals[a]	13.9	1.0	4.3	9.9	2.4	4.3
χ_{CH_3OH}	0.501	0.321	0.352	0.480	0.263	0.212
$\chi_{(CH_3)_2O}$	0.896	0.638	0.629	0.586	0.921	0.931

[a] Higher hydrocarbons and coke (calculated on the basis of C_2H_4).

the CrAPSO-44 sample retains the lowest quantity of methanol. Figure 4 shows that the CrAPSO-44 sample has a much lower temperature DME desorption peak than would be expected if Cr^{3+} was incorporated into the framework forming the characteristic Cr–O interatomic distance. In fact, the DME desorption peak temperature for this sample is practically the same as that for the CrAPSO-34 sample, which also exhibits a relatively low quantity of retained methanol (see Table 2 in Ref. (*8*)). This lack of correlation between the DME desorption peak temperature and the Cr–O interatomic distance as well as the similarities in the TPD spectra of the CrAPSO-44 and SAPO-44 samples lead us to the conclusion that Cr^{3+} is not incorporated into the framework. Instead, it forms species that block part of the active centers of the catalyst. Table 2 also shows that the $AlPO_4$-5 sample has some Brønsted acidity, but not strong enough to catalyze dehydration of methanol to olefins. $AlPO_4$-14 must have very weak acidic groups that cannot retain methanol after degassing at room temperature, thus giving no TPD spectrum. However, as the data on the reaction rates given in Table 4 demonstrate, these

TABLE 4

The Concentration of Active Centers in Catalysts, T–O Distances of Isomorphously Substituted Elements Forming the Active Centers, TPD Peak Temperatures for Dimethylether Desorption, Molar Ratio of Desorbed Dimethylether to Desorbed Methanol, and Reaction Rates for Methanol Dehydration at 623 K and 0.18 MPa

Sample	Conc. of el. (mol/g cat)	d_{T-O} (Å)	T_{des} (K)	DME/M	Reac. rate (mol/g h)
SAPO-44	2.31E-3(Si)	1.62(Si-O)	408	0.053	0.13
CoAPSO-44	0.65E-3(Co)	1.94(Co-O)	487	0.082	0.10
MnAPSO-44	0.65E-3(Mn)	2.02(Mn-O)	510	0.102	0.08
CrAPSO-44	0.17E-3(Cr)	1.84(Cr-O)	418	0.186	n.d.
ZnAPSO-44	0.65E-3(Zn)	1.96(Zn-O)	483	0.015	n.d.
MgAPSO-44	0.66E-3(Mg)	0.88(Mg-O)	468	0.010	n.d.
$AlPO_4$-5	—	—	—	—	0.13
$AlPO_4$-14	—	—	—	—	0.28

TABLE 5

Ethene Selectivities Obtained from TPD and Catalytic Measurements

Sample	Selectivity toward C_2H_4 (C-wt%)	
	TPD	CST reactor
SAPO-44	30.8	18.6
CoAPSO-44	52.5	33.7
MnAPSO-44	35.2	19.3
CrAPSO-44	21.4	n.d.
ZnAPSO-44	42.3	n.d.
MgAPSO-44	19.8	n.d.
$AlPO_4$-5	0.0	0.0
$AlPO_4$-14	0.0	0.0

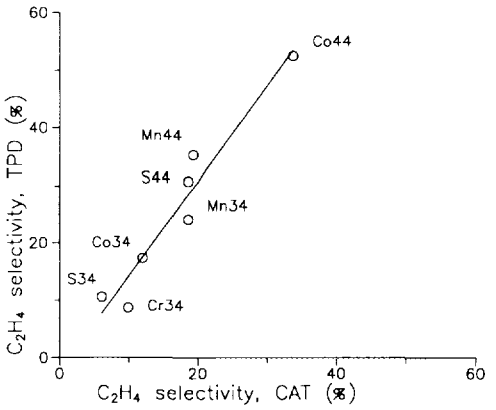

FIG. 5. Linear relationship between the ethene selectivities determined from TPD and catalytic measurements.

two samples have appreciable catalytic activity for the first step of methanol dehydration to DME.

The comparison of data on reaction rates given in Table 4 with data on reaction rates given in Table 4 of our preceding paper (*8*) reveals that catalytic activity in methanol dehydration does not depend on the structural type of the aluminophosphate-based molecular sieves, but it depends slightly on the type of transition metal incorporated into the framework (i.e., Co or Mn). These data also demonstrate that the higher the acidity strength of the sample, the lower is the overall reaction rate of methanol dehydration.

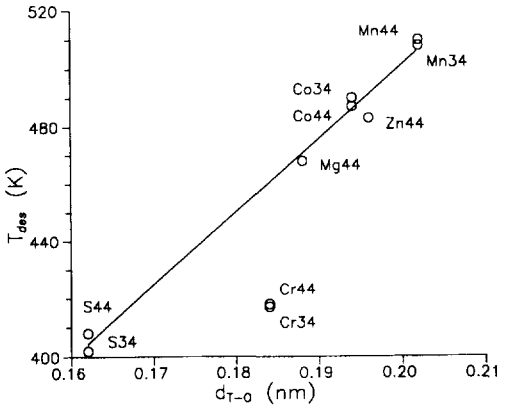

FIG. 4. Linear relationship between the temperature of DME desorption peak and T–O interatomic distance (T = Si, Co, Mn, Cr, Zn, Mg).

However, in the case of selectivities of the samples toward ethene formation the situation is quite different. First, it is interesting to note a very good linear relationship between the selectivities determined from TPD data (*8*) and those determined from the measurements of reaction rates in the gradientless catalytic reactor. This relationship is shown in Fig. 5. Such a result gives us confidence that the *relative* selectivities calculated from TPD data have the same order as those determined from catalytic measurements. Second, comparing the data on selectivity given in Table 5 with those given in Table 5 of the preceding paper (*8*), one can see that the samples having the -44-type structure are about three times more selective for ethene production than those having the -34-type structure. However, simultaneously the type of the metal incorporated into the framework of the particular structural type of molecular sieve also influences strongly the selectivity, as can be seen in Fig. 6. The difference in selectivity to ethene between the MeAPSO-34 and MeAPSO-44 series cannot be explained by the difference in the size of crystals. From the

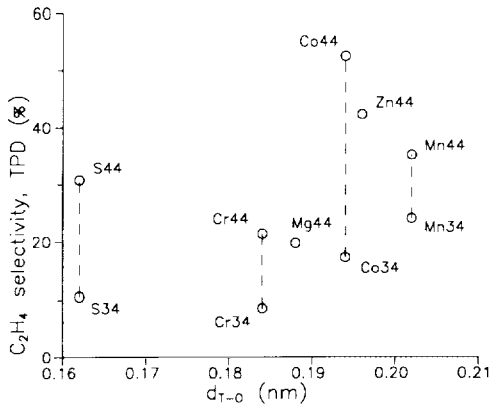

FIG. 6. Relationship between the ethene selectivity determined from TPD measurements and T–O interatomic distance for the SAPO-34, MeAPSO-34 and SAPO-44, MeAPSO-44 structural type samples.

SEM micrographs of the as-synthesized CoAPSO-34 and CoAPSO-44 samples shown in Figs. 7a and 7b one can conclude that the crystal sizes of both samples are comparable. Therefore the difference in selectivity can be ascribed only to the differences in structure between the two homologous series. Using the published crystallographic data of as-synthesized CoAPSO-34 (*6*) and CoAPSO-44 (*7*) samples we generated both stereoplots by the ORTEP program and extracted two equivalent 8-membered rings shown in Fig. 8. The mean of the squares of the four distances between the centers of oxygen atoms in diagonal positions, diminished by the doubled oxygen ion radius (0.244 nm), characteristic for these structures (*15*), gives the mean diameter of the 8-membered ring aperture. The values of this diameter for both structural types is given in Table 6 together with the kinetic diameters of the reactant and product molecules (*16*). Since the frameworks of aluminophosphate molecular sieves can change significantly upon calcination the unit cell parameters of as-synthesized and calcined CoAPSO-34 and CoAPSO-44 samples were compared (Table 7). As can be seen, the unit cell parameters of the CoAPSO-44 sample do not change much after calcination, while the parameter c and the unit cell volume of the CoAPSO-34 sample are substantially reduced after calcination. The unit cell volume of the CoAPSO-34 sample "shrinks" after calcination for about 100 Å^3. If we make a reasonable assumption that the T–O bond distances and bond angles do not change much due to calcination, then the only other explanation is that the conformation of the 8-membered rings in calcined CoAPSO-34 changes. In that sense the apertures of the 8-membered rings in the calcined CoAPSO-34 sample

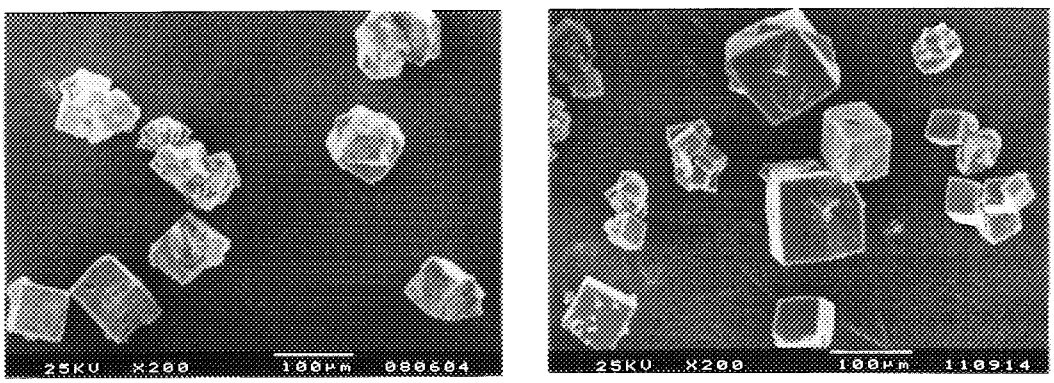

FIG. 7. SEM micrographs of as-synthesized molecular sieves: (left) CoAPSO-34; (right) CoAPSO-44.

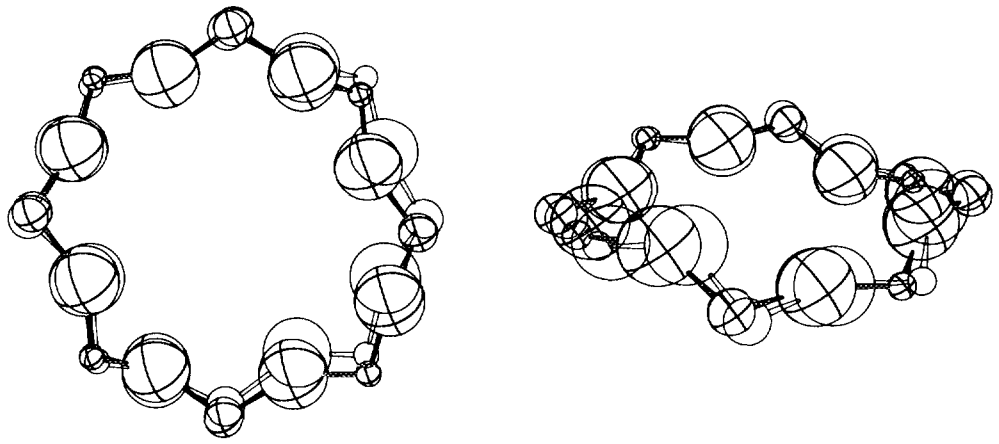

FIG. 8. ORTEP projections of 8-membered rings in CoAPSO-34 and CoAPSO-44 structures: (a) in-plane projection with one common position of oxygen atoms in both structures (left side of the picture); (b) projection rotated for 70° out of plane. Crossed balls represent CoAPSO-34, plain balls represent CoAPSO-44; large balls, oxygen, medium-sized balls, aluminium; small balls, phosphorus.

would be even smaller than the reported value of 0.430 nm in Table 6, calculated from the single crystal X-ray diffraction data of the as-synthesized sample.

The detailed mass balance data given in Table 3 in this and in the preceding paper (*8*) clearly reveal differences between -44 and -34 structures in the *selectivity to product* behaviour. While the quantities of DME and ethene among desorbed species are substantially higher for -44 structures, the quantity of residuals (higher hydrocarbons and coke) is, on the contrary, higher for -34 structures. From these data and from the data of Tables 6 and 7 it is clear that once DME is formed in the chabazite-like cages of both structural types, it can hardly leave these cages since its kinetic diameter is very close to the 8-membered ring aperture. Therefore, it will be transformed instead on the strongly acidic Brønsted centers into ethene. Once ethene is formed, its diffusion out of the chabazite-like cages, through the 8-membered ring apertures, would be easier in the -44-type structure than in the -34-type structure. The restricted diffusion of ethene from the -34- type structure prolongs its residence time within the cage and favors its

TABLE 6

Sizes of 8-Membered Ring Apertures in CoAPSO-34 and CoAPSO-44 Structures and Kinetic Diameters of Reactant and Product Molecules

Reactant and products	σ_k (nm)	8-Membered ring aperture (nm)
Water	0.264	
Methanol	0.363	
Ethene	0.416	0.430 (CoAPSO-34)
Dimethylether	0.431	0.439 (CoAPSO-44)
Ethane	0.444	
Propene	0.468	

TABLE 7

Unit Cell Parameters of As-Synthesized and Calcined CoAPSO-34 and CoAPSO-44 Samples

Sample	CoAPSO-34	CoAPSO-44
As-synthesized		
$a = b$ (Å)	13.804(4)	13.599(2)
c (Å)	14.898(8)	15.302(4)
V (Å)^3	2458	2451(1)
Calcined		
$a = b$ (Å)	13.587(5)	13.602(8)
c (Å)	14.762(8)	15.29(2)
V (Å)^3	2360(3)	2449(6)

transformation through oligomerization reactions to higher hydrocarbons and subsequently to coke. Hence, the very subtle difference in the shape and mean diameter of the 8-membered ring apertures between the two structural types lies at the origin of the difference in the selectivity for ethene in the methanol dehydration reaction.

Among the samples with -44-type structure the most selective for ethene is CoAPSO-44. As can be seen from Fig. 6, there is no simple correlation between the selectivity to ethene and the T–O distance within the isostructural series. Since there is also no simple correlation between the quantity of adsorbed methanol and the loading of silicon and/or metal in the aluminophosphate-based matrix (*vide infra*), one has to conclude that the adsorption and selectivity properties may depend also on other factors such as the oxidation state of the metal in the framework and its coordination. These two factors are however connected with the *d*-character of the transition metals in question.

As in the case of SAPO-34 and MeAPSO-34 samples (*8*), the molar fraction of desorbed water during the TPD of methanol from SAPO-44 and MeAPSO-44 samples is much higher than expected on the basis of the methanol dehydration reaction stoichiometry. The first quantities of water begin to desorb simultaneously with unconverted methanol. This effect was ascribed by us (*8*) to the fast surface-exchange reaction (*17*) between loosely bonded methanol and strongly bonded water that remained undesorbed during the vacuum/heat pretreatment of the molecular sieves before the introduction of dry methanol into the adsorption vessel. At least two more peaks of desorbed water appear then at higher temperatures. One occurs immediately *before* the desorption of DME and the other immediately *before* the desorption of hydrocarbon species (i.e., ethene). These water desorption peaks are connected with the successive dehydration steps of methanol to DME and DME to hydrocarbons, respectively, in accordance with the sequence of products appearance as the function of reaction temperature during the catalytic dehydration of methanol (*8*). The stepwise release of water during TPD is evident on CoAPSO-44 (see Fig. 2), MgAPSO-44, MnAPSO-44, and ZnAPSO-44 samples. Most clearly it can be followed on MgAPSO-44 because the quantity of methanol that remains adsorbed after degassing of the sample at 293 K before the onset of TPD process is the highest among all the samples (see Table 2).

The release of water *before* DME and hydrocarbons (i.e., ethene) during the TPD process indicates that DME, as the reaction intermediate, and hydrocarbons, as the products (especially unsaturated ones), are held more strongly on the active sites than water. If the interaction of these molecules with adsorption centers would be polar in character, the sequence of desorption would be reversed, since the electric dipole moments of DME, methanol and water are 1.30, 1.70, and 1.85 Debyes, respectively (*18*). If, however, the interaction would be of the donor–acceptor type, i.e., if these molecules behave as ligands, then the sequence of desorption would follow the donating ability sequence of the ligands. In general, a donor atom in the ligand will have greater ability to form complexes if it has higher negative charge. According to Sanderson (*19*), the negative charges on the oxygen atom in DME, methanol and water are as follows: -0.31, -0.29, and -0.25, respectively. Therefore, one can expect that DME would be the strongest ligand among these molecules. The view, according to which the metals, incorporated into the aluminophosphate framework, behave as coordinatively unsaturated species (see for instance Ref. (*4*), does not look very strange if we keep in mind the crystal field stabilization energies (CFSE) of these metals in different coordinations (*20*), and the fact that the aluminophosphate frameworks in question (i.e., -34 and -44 types) can figure at most as quadridentate ligands, coordina-

tively saturating only those elements that are stable in tetrahedral coordination. For elements whose CFSE is higher in octahedral than in tetrahedral coordination, secondary ligands would be needed in order to saturate them coordinatively. Water, methanol, and DME can serve for this purpose. If so, the quantity of methanol retained on molecular sieves after degassing should be higher on samples containing metal ions with a preference for higher than tetrahedral coordination. Indeed, the data in Table 2 corroborate this way of thinking, since the quantity of retained methanol is not proportional to the framework charge of the samples (see Table 1).

The discussion presented above can shed some light on the great differences in the selectivity for ethene formation between the samples containing transition metal ions within the isostructural homologue series (i.e., within MeAPSO-44 series) that could not be correlated either with T–O distances, or with the acidity strength sequence. Namely, the stabilities of transition metal–ligand complexes usually vary in the Irving–Williams order: $Mn^{II} < Fe^{II} < Co^{II} < Ni^{II} < Cu^{II} > Zn^{II}$ irrespective of the type of ligand (*20*). This order is the consequence of the extra stability of complexes due to the contribution of the CFSE of the atomic *d*-orbitals to the ligation energy. If the ligation energy of ethene (π-complex) with transition metal is higher, it will be less prone to the subsequent oligomerization reaction leading to coke formation, and, consequently, such a catalyst would be more selective to ethene. If this is true, then NiAPSO-*n* samples should be the most selective ones for ethene, since Ni- complexes have the highest CFSE. At least two publications in the recent literature do indeed claim the very high selectivity to ethene of NiAPSO-34 samples in the methanol dehydration reaction (*3*, *4*).

CONCLUSIONS

Using two isostructural series of homologues (MeAPSO-44 and MeAPSO-34) with the same isomorphously substituted elements, we succeeded to decouple the effect of isomorphously substituted transition elements and the effect of molecular shape-selectivity to product on the overall selectivity to ethene in the methanol dehydration reaction. Two rather important results concerning the catalysis on transition metal substituted silicoaluminophosphate molecular sieves follow from this study.

(a) In a given homologous series the selectivity to ethene in the methanol dehydration reaction follows the Irving–Williams order of the stabilities of transition metal–ligand complexes. This is an example of the linear free energy relationship (LFER) between a structure-insensitive property of the catalyst (i.e., *d*-character of transition metal) and the selectivity in a given reaction.

(b) Almost a threefold difference in selectivity to ethene between MeAPSO-44 structural type homologues and MeAPSO-34 structural type homologues is due to the difference in molecular shape-selectivity to product caused by the small difference in the dimensions of the 8-membered ring apertures.

ACKNOWLEDGMENTS

Financial support of the Ministry of Science and Technology (MZT), Grant C2-0538-104, is gratefully acknowledged.

REFERENCES

1. Inui, T., Matsuda, H., Okaniwa, H., and Miyamoto, A., *Appl. Catal.* **58,** 155 (1990).
2. Liang, J., Li, H., Zhao, S., Guo, W., Wang, R., and Ying, M., *Appl. Catal.* **64,** 31 (1990).
3. Inui, T., Phatanasri, S., and Matsuda, H., *J. Chem. Soc. Chem. Commun.*, 205 (1990).
4. Thomas, J. M., Xu, Y., Catlow, C. R. A., and Couves, J. W., *Chem. Mater.* **3,** 667 (1991).
5. Ito, M., Shimoyama, Y., Saito, Y., Tsurita, Y., and Otake, M., *Acta Crystallogr. Sect. C* **41,** 1698 (1985).
6. Bennett, J. M., and Marcus, B. K., *Stud. Surf. Sci. Catal.* **37,** 269 (1988).
7. Nardin, G., Randaccio, L., Kaučič, V., Rajić, N., *Zeolites* **11,** 192 (1991).

8. Hočevar, S., and Levec, J., *J. Catal.* **135,** 518 (1992).
9. Lok, B. M. T., Messina, C. A., Patton, R. L., Gajek, R. T., Cannan, T. R., and Flanigen, E. M., U.S. Patent 4,440,871 (1984).
10. Lok, B. M. T., Marcus, B. K., and Flanigen, E. M., EP 0 161 489 (1985).
11. Lok, B. M. T., Marcus, B. K., and Flanigen, E. M., EP 0 161 490 (1985).
12. Lok, B. M. T., Vail, L. D., and Flanigen, E. M., EP 0 158 975 (1985).
13. Flanigen, E. M., Lok, B. M. T., Patton, R. L., and Wilson, S. T., U.S. Patent 4,738,837 (1988).
14. Wilson, S. T., Lok, B. M. T., Flanigen E. M., EP 0 043 562 (1982).
15. Flanigen, E. M., Patton, R. L., and Wilson, S. T., *Stud. Surf. Sci. Catal.* **37,** 13 (1988).
16. Reid, R. C., Prausnitz, J. M., and Poling, B. E., "The Properties of Gases and Liquids," 4th ed., p. 733. McGraw–Hill, New York, 1987.
17. Rozovskii, A. Ya., *Kinet. Katal.* **30,** (3), 533 (1989).
18. "CRC Handbook of Chemistry and Physics," 53rd ed., p. E51. The Chemical Rubber Co., Cleveland, Ohio, 1972.
19. Sanderson, R. T., "Inorganic Chemistry," p. 105. Reinhold, New York, 1967.
20. Greenwood, N. N., and Earnshaw, A., "Chemistry of the Elements," p. 1060. Pergamon, Oxford, 1984.